BAMS Article

Tropical Cyclone Precipitation, Infrared, Microwave, and Environmental Dataset (TC PRIMED)

Muhammad Naufal Razin, Christopher J. Slocum, John A. Knaff, Paula J. Brown, and Michael M. Bell

KEYWORDS: Precipitation; Tropical cyclones; Satellite observations; Diagnostics; Reanalysis data

ABSTRACT: To study tropical cyclones and generate forecast applications using satellite observations, researchers often consolidate disparate sources of raw and ancillary data. Data consolidation involves obtaining, collocating, and intercalibrating data from different sensors and derived products; calculating environmental diagnostics from a homogeneous source; and standardizing these various products for a straightforward analysis. To alleviate preprocessing issues and provide a long-term, global digital dataset of tropical cyclone satellite observations, we construct the Tropical Cyclone Precipitation, Infrared, Microwave, and Environmental Dataset (TC PRIMED). TC PRIMED contains tropical cyclone–centric 1) intercalibrated, multichannel, multisensor microwave brightness temperatures, 2) retrieved rainfall from NASA's Goddard Profiling Algorithm (GPROF), 3) nearly coincident geostationary satellite infrared brightness temperatures and derived metrics, 4) tropical cyclone position and intensity information, 5) ECMWF fifth-generation reanalysis fields and derived environmental diagnostics, and 6) precipitation radar observations from the TRMM and GPM *Core Observatory* satellites. TC PRIMED consists of over 176,000 overpasses of 2,101 storms from 1998 to 2019, providing researchers with an analysis-ready dataset to promote and support research into improving our understanding of the relationship between tropical cyclone convective and precipitation structure, intensity, and environment. Here, we briefly describe data sources and processing steps to create TC PRIMED. To demonstrate TC PRIMED's potential utility for studying important tropical cyclone processes and for application development, we present a shear-relative composite analysis of several multisensor satellite variables relative to the tropical cyclone lifetime maximum intensity. The composite analysis provides a simple example of how TC PRIMED can benefit future studies to advance our understanding of tropical cyclones and improve forecasts.

https://doi.org/10.1175/BAMS-D-21-0052.1
Corresponding author: Naufal Razin, naufal@colostate.edu
Supplemental material: https://doi.org/10.1175/BAMS-D-21-0052.2
In final form 1 July 2022

AFFILIATIONS: Razin—Department of Atmospheric Science, Colorado State University, and Cooperative Institute for Research in the Atmosphere, Fort Collins, Colorado; **Slocum and Knaff**—NOAA/Center for Satellite Applications and Research, Fort Collins, Colorado; **Brown and Bell**—Department of Atmospheric Science, Colorado State University, Fort Collins, Colorado

Tropical cyclones cause massive property damage and loss of life worldwide. Their significant impacts continue to motivate studies to better understand the relationships between the tropical cyclone environment, convective and precipitation structure, and intensity—factors that influence how hazards such as strong winds, storm surges, and heavy rainfall affect communities. Researchers have often used satellite observations to observe and analyze tropical cyclones in a diverse set of environments, due in part to limitations of conventional ground-based observations. Satellite observations from passive microwave sensors are particularly useful for tropical cyclone forecasting and research, as they can peer through cloud tops and provide insight into the convective and precipitation structure of tropical cyclones.

The tropical cyclone community has used satellite passive microwave observations to advance our understanding of tropical cyclone evolution, intensity, and structure, and improve forecasts. Among the various sources of tropical cyclone passive microwave observations available to the community, the most prominent is the NRL Tropical Cyclone website (Hawkins et al. 2001). NRL TC aids in forecasts by supplying near-real-time imagery in operationally useful channels (e.g., 37 and 85–92 GHz) from various sensors with other satellite-based products (e.g., visible, infrared, and water vapor channels). To conduct research, the community can obtain publicly available digital datasets from sources such as the HURSAT-MW (Knapp 2008), the Tropical Cyclone Precipitation Feature database (Jiang et al. 2011), or products from the NASA JPL Tropical Cyclone Information System (Hristova-Veleva et al. 2020). In addition, researchers have used large private datasets of tropical cyclone passive microwave observations to investigate the various aspects of tropical cyclones (e.g., Lonfat et al. 2004; Jones et al. 2006; Wingo and Cecil 2010; Harnos and Nesbitt 2011; Cossuth 2014; Alvey et al. 2015; Rozoff et al. 2015). We present a more extensive summary of previous work in the online supplemental document, "TC PRIMED: A summary of previous work" (https://doi.org/10.1175/BAMS-D-21-0052.2).

However, these datasets are either not publicly available, consists of a limited set of sensors with uncalibrated data or contain limited information on the tropical cyclone and its environment. Therefore, the scientific community would benefit from an open-access, long-term, global, and standardized digital dataset of multisensor passive microwave observations of tropical cyclones. This dataset would contain intercalibrated microwave brightness temperatures, retrieved rainfall, coincident infrared brightness temperatures, tropical cyclone information such as track and intensity, and a full suite of tropical cyclone environmental information from a single, consistent source. Considering that such a dataset requires a monumental effort to compile, it does not exist—until now.

We have compiled a comprehensive global, multisensor passive-microwave-based digital dataset of tropical cyclones with best track, environmental diagnostics, and reanalysis data known as the Tropical Cyclone Precipitation, Infrared, Microwave, and Environmental Dataset (TC PRIMED). TC PRIMED contains tropical cyclone–centric 1) intercalibrated, multichannel,

multisensor microwave brightness temperatures from low-Earth-orbit (LEO) satellites, 2) retrieved rainfall from NASA's Goddard Profiling Algorithm (GPROF), 3) nearly coincident infrared (IR) brightness temperatures from geostationary satellites (GEO) with IR-based metrics, 4) tropical cyclone position and intensity information, 5) ECMWF fifth-generation reanalysis (ERA5) fields and derived environmental diagnostics, and 6) precipitation radar observations from the Tropical Rainfall Measurement Mission (TRMM) and Global Precipitation Measurement (GPM) *Core Observatory* satellites. With TC PRIMED's unique dataset of over 176,000 LEO satellite overpasses of 2,101 storms from 1998 to 2019, we eliminate the tremendous effort needed to ensure consistency and ease of use of the data by standardizing the different data sources and formats, and obtaining environmental and diagnostic data from a single, homogeneous source. With an all-encompassing dataset, the scientific community can focus on conducting studies of the tropical cyclone environment, convective and precipitation structure, and intensity.

Here, we discuss the data sources and processing steps employed to create TC PRIMED. To highlight the utility of TC PRIMED, we present a brief shear-relative composite analysis of satellite parameters. Then, we summarize this work and offer concluding remarks. For a list of key abbreviations and acronyms, we refer readers to the appendix.

Data sources and description

The primary component of TC PRIMED is LEO observations. We prioritize LEO observations from passive microwave sensors and precipitation radars to capitalize on their ability to infer various atmospheric properties such as precipitation. However, we supplement the LEO observations with gridded geostationary longwave IR window channel observations near 11 μm, environmental diagnostic variables, and reanalysis fields. These different components of TC PRIMED have their own data sources but are stored locally at CSU and CIRA, making the compilation process straightforward. We discuss the data source for each TC PRIMED component below and present how we organize these components in TC PRIMED files in the following section. While we document the data source information such as the data version, processing levels, and DOIs in the metadata section of each TC PRIMED file, interested readers can also refer to the supplemental document, "TC PRIMED: Data source documentation."

We obtain LEO data from the NASA GPM constellation satellites (Hou et al. 2014). The GPM constellation consists of satellites from NASA's domestic and international partners, with the partnerships formed through bilateral agreements. While each partnering agency launched their satellites with its own unique scientific and weather-monitoring objectives, the members of the partnership consolidated their data to develop a set of global microwave-based intercalibrated brightness temperature and precipitation observations for the GPM mission. The GPM mission generates intercalibrated microwave brightness temperatures for each constellation satellite using the GPM satellite as the "Core Observatory" for bias assessments and to provide adjustments. The intercalibration process is complex but necessary to correct sensor biases that can be as little as 2–3 K to as large as 7–11 K (Berg et al. 2016). Thus, the intercalibration process ensures a long-term record of microwave brightness temperatures that are consistent with the GPM Microwave Imager (GMI) aboard the GPM *Core Observatory* such that the differences in the brightness temperatures between the constellation sensors are mainly due to differences in the observing frequencies and sensor characteristics.

For TC PRIMED, we use version 5 of the NASA level 1C intercalibrated microwave brightness temperature data from sensors that have a long enough record to allow for intercalibration, and enough channels to provide meaningful precipitation estimates. Figure 1 shows a list of intercalibrated microwave frequencies and polarizations for each sensor included in TC PRIMED. Note that some channels are not available in this version of TC PRIMED since

AMSR2 & AMSR-E	AMSU-B	ATMS	GMI
10.65 V & H 18.7 V & H 23.8 V & H 36.5 V & H 89.0 V & H	89.0±0.9 QV 150.0±0.9 QV 183.31±1.0 QV 183.31±3.0 QV 183.31±7.0 QV	23.8 QV 31.4 QV 88.2 QV 165.5 QH 183.31±1.0 QH 183.31±1.8 QH 183.31±3.0 QH 183.31±4.5 QH 183.31±7.0 QH	10.65 V & H 18.7 V & H 23.8 V 36.64 V & H 89.0 V & H 166.0 V & H 183.31±3.0 V 183.31±7.0 V
MHS	**SSM/I**	**SSMIS**	**TMI**
89.0 V 157.0 V 183.31±1.0 H 183.31±3.0 H 190.31 V	19.35 V & H 22.235 V 37.0 V & H 85.5 V & H	19.35 V & H 22.235 V 37.0 V & H 91.665 V & H 150.0 H 183.31±1.0 H 183.31±3.0 H 183.31±6.6 H	10.0 V & H 19.35 V & H 21.3 V 37.0 V & H 85.5 V & H

Fig. 1. List of microwave frequencies (in GHz) and polarizations available for each sensor in TC PRIMED. V, H, QV, and QH refer to the respective vertical, horizontal, quasi-vertical, and quasi-horizontal polarizations.

the GMI does not have similar channels that would allow for intercalibration (e.g., 50–60-GHz channels from the SSMIS).

The spaceborne radar data in TC PRIMED come from the GPM (Hou et al. 2014) and the TRMM (Kummerow et al. 1998) *Core Observatory* satellites. The GPM satellite carries the Dual-Frequency Precipitation Radar (DPR) to measure precipitation in the Ku and Ka band, or 13.6 and 35.5 GHz, respectively. While the DPR has a higher spatial resolution (5 km) compared to the variable instantaneous fields of view (IFOV) in the various microwave frequencies, it has a narrower swath width (245 km) than the microwave imager (885 km; Hou et al. 2014). TC PRIMED uses version 6 of the NASA level 2B GPM DPR combined radar–radiometer data, which combines observations from the GPM DPR and GMI to derive the hydrometeor and precipitation information in the GPM DPR swath (Grecu et al. 2016). However, radar observations such as reflectivity and precipitation type come solely from the GPM DPR (Olson et al. 2018). The GPM DPR's predecessor, the TRMM Precipitation Radar (PR), measures precipitation only in the Ku band and has a similarly narrower swath width compared to that of its imager. Similar to the GPM DPR, we use version 6 of the NASA level 2B combined TMI–PR data for TC PRIMED.

Passive-microwave-based precipitation data in TC PRIMED come from NASA's GPROF (Kummerow et al. 2015). GPROF generates estimates of precipitation using a Bayesian scheme to weight a database of GMI brightness temperatures and footprint-averaged rain rates and hydrometeor profiles from the GPM combined radar–radiometer product. The database comes from one year of global observations—excluding over snow-covered surfaces—and organized by surface type, total column water vapor, and 2-m temperature. To simulate the brightness temperatures for the different constellation sensors, GPROF uses a radiative transfer model. Therefore, each GPM constellation sensor has its own specific database of brightness temperatures and corresponding hydrometeor profiles. For TC PRIMED, we use version 5 of the NASA level 2A-CLIM GPROF data. The level 2A-CLIM data differ from the level 2A data in that they uses ancillary data from the ECMWF reanalysis. By using the

GPROF precipitation estimates, TC PRIMED provides a consistent precipitation product for each GPM constellation sensor. In compiling TC PRIMED, we also retain the original swath grids of the LEO observations (i.e., NASA level 1 and level 2; NASA Earthdata 2021).

Since extreme events are naturally infrequent and are not well-represented in Bayesian schemes, GPROF generally underestimates extreme events that can occur in tropical cyclones. While a GPROF algorithm specific to tropical cyclones would yield better precipitation estimates in tropical cyclones (HGPROF; Brown et al. 2016), such an algorithm is not widely available for the GPM constellation sensors throughout the TC PRIMED period. Therefore, we compile TC PRIMED with the generalized version of GPROF.

For the gridded geostationary IR data in TC PRIMED, we use data from two sources: 1) the HURSAT dataset (Knapp and Kossin 2007) and 2) the RAMMB/CIRA IR archive (Knaff et al. 2016, 2019). The HURSAT dataset contains 3-hourly, 8-km IR brightness temperatures while the RAMMB/CIRA dataset contains 4-km IR brightness temperatures at a higher temporal resolution—both remapped to a Mercator projection. The HURSAT dataset has a much longer historical record, especially in the western North Pacific, Indian Ocean, and Southern Hemisphere basins.

In addition to the IR data, we include several IR-based products. One product is tropical cyclone size information developed by Knaff et al. (2014, 2017). Knaff et al. (2014, 2017) defined the tropical cyclone size as the radius at which the azimuthal mean tangential wind speed at the 850-hPa level is 5 kt (1 kt = 0.514 m s^{-1}) (R5), which they assumed is indistinguishable from the background winds. Using the 5-kt threshold ensures that all storms regardless of intensity have a defined size metric. To retrieve the value of R5, Knaff et al. (2014, 2017) used azimuthally averaged IR brightness temperature patterns, storm intensity, latitude, and climatological storm size parameters. This method provides a tropical cyclone size estimate simply from IR observations and storm intensity estimates—both of which are routinely available. Besides providing tropical cyclone size information, retrieved R5 values can serve as a scaling factor when combined with the climatological value of R5 (R5c), which is a function of tropical cyclone intensity. The scaling factor scales the observations to account for the different tropical cyclone sizes such that storms with a climatologically small wind field will have a scaled radius larger than its physical radius, while the reverse is true for storms with a climatologically large wind field. We offer a more detailed discussion on the retrieval of R5 and the radius scaling in the supplemental document, "TC PRIMED: Radius scaling in satellite composites."

Another set of IR-based products that we include in TC PRIMED is the IR predictors used in the Statistical Hurricane Intensity Predictions Scheme (SHIPS; DeMaria and Kaplan 1994; DeMaria et al. 2005). These predictors use the IR data to describe the state of the tropical cyclone using variables such as mean and standard deviation of IR brightness temperatures between the 0–200-km annulus and the 100–300-km annulus, and percent areal coverage of brightness temperature pixels below various thresholds from −10° to −60°C.

For estimates of storm location and intensity, we use the tropical cyclone final postseason best track database files of the Automated Tropical Cyclone Forecast system (ATCF; Sampson and Schrader 2000). By design, the ATCF best track is a smoothed record of tropical cyclone location, intensity, and other parameters from information generated by the National Hurricane Center, the Central Pacific Hurricane Center, and the Joint Typhoon Warning Center at the 6-hourly intervals corresponding to the standard synoptic times (0000, 0600, 1200, and 1800 UTC). These operational tropical cyclone centers use the same maximum sustained 1-min wind conventions for intensity estimation, providing a consistent source of tropical cyclone intensity information for TC PRIMED. Note that while the storm location and intensity come from a single source, the best track data have well-documented inconsistencies in time due to changes in observing systems (Landsea et al. 2010) and uncertainties in

quantities (Landsea and Franklin 2013; Knaff et al. 2021) that users should consider when using TC PRIMED. We provide metadata in TC PRIMED that help users navigate around these discrepancies.

To represent the tropical cyclone environment, we include diagnostic quantities commonly available to—and used by—the tropical cyclone community. This suite of environmental quantities characterizes the thermodynamic, dynamic, and kinematic fields around the storm using a single value at each observation time and—for vertical profiles—at each vertical level. Each quantity derives from azimuthally averaging the fields within an annulus around the center of the storm. Different diagnostic quantities have a different set of vertical levels and annulus regions with which they are calculated, and these vertical levels and annulus regions are standard to the tropical cyclone community. For example, one type of vertical shear quantity involves calculating the difference between the 850- and 200-hPa-level wind velocities, azimuthally averaged between the 0–500-km annulus. Another type of shear quantity involves the same wind velocity difference, but azimuthally averaged between the 200–800-km annulus. These environmental diagnostic quantities serve as input to statistical–dynamical models like the SHIPS Developmental Dataset. However, while these diagnostic quantities are available to the community in the SHIPS Developmental Dataset, the SHIPS Developmental Dataset combines the operational version of the Global Forecast System with the Climate Forecast System Reanalysis (RAMMB 2020). Therefore, the developmental version contains inhomogeneities due to model upgrades. To ensure consistency throughout the TC PRIMED period, we calculate the environmental model diagnostic quantities from ERA5 (Hersbach et al. 2020). We refer the reader to Slocum et al. (2022) for an overview of the averaging regions for each diagnostic quantity, and for a detailed comparison of the environmental diagnostics calculated in ERA5 and the SHIPS Developmental Dataset.

ERA5 consists of hourly analyzed fields. However, we calculate the environmental diagnostics at each synoptic time (0000, 0600, 1200, and 1800 UTC) in the best track database during the storm's life cycle. We obtain the reanalysis outputs from the European Union's Copernicus Climate Change Service on pressure- and single-level surfaces at a uniform 0.25° horizontal grid spacing (Hersbach et al. 2018a,b). In addition to the calculated diagnostic quantities, we also include pertinent gridded ERA5 fields on their native output grids. The ERA5 fields are available at the surface level, and from the 1,000-hPa level to the 100-hPa level at every 50 hPa, with the addition of the 975- and 925-hPa levels. Relevant diagnostic fields also have the same vertical resolution.

Processing steps

We organize TC PRIMED files by year, basin, and storm directories. In each storm directory, two types of files reside: 1) an overpass file and 2) an environmental file. An overpass file contains the satellite-specific variables associated with one satellite overpass, whereas an environmental file contains the best track information, environmental diagnostics, and gridded ERA5 variables at each synoptic time throughout the storm's life cycle. Therefore, for each storm, multiple overpass files exist, of which the exact number depends on various factors such as the storm duration and the number of satellites in orbit. Conversely, there would be only one environmental file for each storm. Both file types are in netCDF format and meet the Climate and Forecast Conventions and Metadata version 1.7 (CF-1.7) and Attribute Convention for Data Discovery version 1.3 (ACDD-1.3) metadata conventions.

Overpass files. We begin compiling TC PRIMED upon the release of the postseason and final best track data by selecting a satellite overpass if the edges of its passive microwave swath traversed within 750 km and ±3 h of the 6-hourly best track storm location. We chose the 750-km distance to focus our dataset on convective and precipitation features that are

relevant to the tropical cyclone. Then, we linearly interpolate the storm's center position to the time of the closest satellite scan. After which, we calculate the satellite coverage within a 750-km radius around the interpolated storm center and retain overpasses with at least 50% coverage. Similarly, we select TRMM PR and GPM DPR data if their swaths are within 750-km radius of the interpolated storm center.

Finally, we adopt a small change to the level 2 rain-type classification algorithm for the TRMM PR and GPM DPR. The original rain-type classification algorithm classifies shallow rain detected by the precipitation radars as convective (Awaka et al. 2016). Shallow rain is precipitation with a storm top that is lower than 1 km below the 0°C level, which is determined from a reanalysis output. Since shallow and nonshallow rain can have vastly different vertical extents and passive microwave signatures, we separate shallow rain from the convective rain type in TC PRIMED to produce five main rain-type categories: no rain, stratiform, convective, other, and shallow rain.

When including IR data for a particular storm, we first determine if the RAMMB/CIRA archive contains any data of the storm. If the RAMMB/CIRA archive contains data of the storm, we search that archive and select the IR data from a single observation that is closest in time and within 3 h of the microwave overpass. If the RAMMB/CIRA archive does not contain any data of the storm, we repeat the steps above with the HURSAT archive. By prioritizing the RAMMB/CIRA IR archive, we include the IR data with the highest spatial and temporal resolution for each overpass in TC PRIMED. In addition, we ensure consistency by selecting IR data from a single source for a particular storm. Since overpasses from multiple satellites can occur close in time, the overpass files from these different satellites may have IR data from the same observation time. For the IR-derived products, we include the R5 values throughout the storm's life cycle in each overpass file. However, the IR-based SHIPS predictors will be based on the single IR observation that we include in each overpass file.

TRMM PR and GPM DPR swaths are not always available due to sporadic instrument failures, nor are they always available within 750 km of the storm center even if their corresponding microwave swaths are within 750-km radius of the storm center. In these cases, we do not include the PR or DPR data in the final overpass file. Similarly, with the exception of the R5 variable, we leave the rest of the IR section of the file empty if no IR data exist within 3 h of the overpass or when no IR data exist at all, which often occurs for the early parts of a storm or storms that were added to the best track following the season. We mark these cases accordingly with a status flag in the overpass file.

Finally, we include intensity and intensity change information in the overpass files. For the intensity, we linearly interpolate the best track intensity to the overpass time. Whereas for the intensity change, we calculate the 6-, 12-, 18-, and 24-h past and future intensity change relative to the overpass time. However, if users are interested to use the overpass file in combination with data from the environmental file—which are available at every synoptic time (0000, 0600, 1200, and 1800 UTC)—we also include the closest synoptic time variable, which enables users to find the environmental variable closest in time to the overpass. Table 1 shows the list of variables that are contained in an overpass file.

Environmental files. After processing the overpass files, we add to the environmental file a list of basic information that includes the overpass file names, sensor names, satellite names, and satellite coverage fractions for each storm. We organize this basic overpass information in order of increasing time. We then include metadata about the storm gathered from the postseason best track ATCF database file and calculate the environmental diagnostics from the ERA5 fields. Slocum et al. (2022) provides a more technical description of the environmental diagnostics calculations using ERA5. However, we summarize the key steps here. To calculate the storm-relative diagnostics, we regrid the ERA5 fields onto a 0–1,500-km cylindrical grid with

Table 1. List of variables and their units that are available in each overpass file. Note that precipitation radar variables are available only on the TRMM or GPM satellite. The list of passive microwave frequencies for each sensor is shown in Fig. 1.

Group	Variable	Units
Overpass metadata	Time	
	Storm latitude	°N
	Storm longitude	°E
	Storm intensity at overpass time	kt
	6-, 12-, 18-, and 24-h past and future intensity change	kt
	Sensor name	
	Satellite name	
	Overpass number	
	Coverage fraction	%
	Closest synoptic time	
	Storm size parameter (R5)	° lat
GPROF	Surface precipitation rate	mm h^{-1}
	Convective precipitation rate	mm h^{-1}
	Rainwater path	kg m^{-2}
	Cloud water path	kg m^{-2}
	Ice water path	kg m^{-2}
	Vertical profile of rainwater	g m^{-3}
	Vertical profile of cloud water	g m^{-3}
	Vertical profile of snow water	g m^{-3}
	Quality flag	
	Surface type	
Passive microwave	Microwave brightness temperatures (see Fig. 1)	K
Precipitation radar (TRMM or GPM)	Status flag	
	Vertical profile of reflectivity	dBZ
	Surface precipitation rate	mm h^{-1}
	Vertical profile of cloud liquid water	g m^{-3}
	Vertical profile of cloud ice water	g m^{-3}
	Vertical profile of precipitation liquid water	g m^{-3}
	Precipitation type	
	Surface type	
Infrared	Status flag	
	Time	
	Brightness temperatures near 11 μm	K
	Annulus mean brightness temperatures	K
	Annulus brightness temperature standard deviation	K
	Areal coverage of brightness temperature thresholds	%

5-km radial × 5° azimuthal grid spacing using bilinear interpolation. This cylindrical grid allows us to calculate the diagnostic quantities within their relevant annulus regions. We center the cylindrical grid on the tropical cyclone center, which we determined using one of two ways: 1) the tropical cyclone center in ERA5 or 2) the best track center when the system is ill-defined (e.g., disturbance, open wave, extratropical transition).

The tropical cyclone center in ERA5 may be different from the observed tropical cyclone center as shown for other reanalysis products (Hodges et al. 2017). Therefore, we locate the ERA5 tropical cyclone center by taking a 4° × 4° box centered on the best track center of the

mean sea level pressure and 850-hPa geopotential height, creating a bivariate spline of each field, and using an optimization algorithm to find the minimum within the domain [see Marchok (2021) for a discussion about fields for vortex position finding]. In cases where we cannot determine the tropical cyclone center in ERA5, such as when the best track position is over land or when the storm's maximum intensity is less than 34 kt (17.5 m s^{-1}), we use the best track center position. Using a quality flag, we specify the method used to obtain the tropical cyclone center for the diagnostics calculation at a particular synoptic time. Then, we calculate the various diagnostic quantities using the cylindrical grid at each synoptic time. Slocum et al. (2022) discuss the sensitivity of the diagnostics values to center location.

Finally, we include pertinent ERA5 fields on their native grid and within 20° latitude × 20° longitude of the storm center in the environmental file. Note that regardless of the number of LEO observations of the storm, the environmental files will always contain data at every synoptic time (0000, 0600, 1200, and 1800 UTC) throughout the storm's life. Table 2 shows the list of variables that are contained in an environmental file.

Table 2. List of key variables and their units that are available in each environmental file. The list is nonexhaustive and excludes variables such as data quality flags.

Group	Variable	Units	Variable	Units
Storm metadata	Time		Best track intensity	kt
	Best track storm latitude	°N	Best track minimum sea level pressure	hPa
	Best track storm longitude	°E	Storm distance to land	km
Overpass metadata	Overpass times		Overpass sensors	
	Overpass file names		Overpass satellites	
	Overpass storm latitude	°N	Overpass number	
	Overpass storm longitude	°E	Overpass coverage fraction	%
Diagnostics	Minimum central sea level pressure	hPa	Vertical profile of temperature	K
	Sea surface temperature	K	Vertical profile of relative humidity	%
	2-m temperature	K	Vertical profile of specific humidity	kg kg^{-1}
	2-m dewpoint temperature	K	Vertical profile of *u*-wind component	m s^{-1}
	10-m *u*-wind component	m s^{-1}	Vertical profile of υ-wind component	m s^{-1}
	10-m υ-wind component	m s^{-1}	Vertical profile of tangential wind component	m s^{-1}
	850–200-hPa shear magnitude	m s^{-1}	Vertical profile of vorticity	s^{-1}
	850–200-hPa shear direction	°	Vertical profile of divergence	s^{-1}
	Precipitable water	kg m^{-2}	Temperature gradient	°C m^{-1}
	Warm-core temperature anomaly	K	Temperature advection	°C s^{-1}
	Convective mass flux	m s^{-1}		
Gridded ERA5	Precipitable water	kg m^{-2}	3D temperature	K
	Large-scale rain rate	kg m^{-2} s^{-1}	3D relative humidity	%
	Convective rain rate	kg m^{-2} s^{-1}	3D specific humidity	kg kg^{-1}
	Sea surface temperature	K	3D *u*-wind component	m s^{-1}
	Mean sea level pressure	hPa	3D υ-wind component	m s^{-1}
	2-m temperature	K	3D vorticity	s^{-1}
	2-m dewpoint temperature	K	3D divergence	s^{-1}
	10-m *u*-wind component	m s^{-1}		
	10-m υ-wind component	m s^{-1}		

Scientific application

Consisting of 2,101 storms worth of combined LEO, GEO, and environmental data, TC PRIMED opens up an avenue for the scientific community to conduct new research without being limited by satellite, sensor, channel, or data consistency and availability. To highlight the value of TC PRIMED, we present an application in the context of Typhoon Sepat (2007). Figure 2 shows observations from a TRMM overpass of Typhoon Sepat at 0223:17 UTC 17 August 2007, as it was undergoing an eyewall replacement cycle off the coasts of the Philippines and Taiwan. Note that while the satellite variables are available within a 750 km × 750 km box around the interpolated storm center, Fig. 2 depicts a closer look of the storm (within ~500 km) to better show the tropical cyclone structures.

From this TRMM satellite overpass, researchers can obtain precipitation information from either GPROF or the combined TMI–PR product, with the surface precipitation rate from both products shown in Figs. 2a and 2b, respectively. Note that the GPROF surface precipitation rate is lower than the TMI–PR surface precipitation rate because GPROF creates an estimate

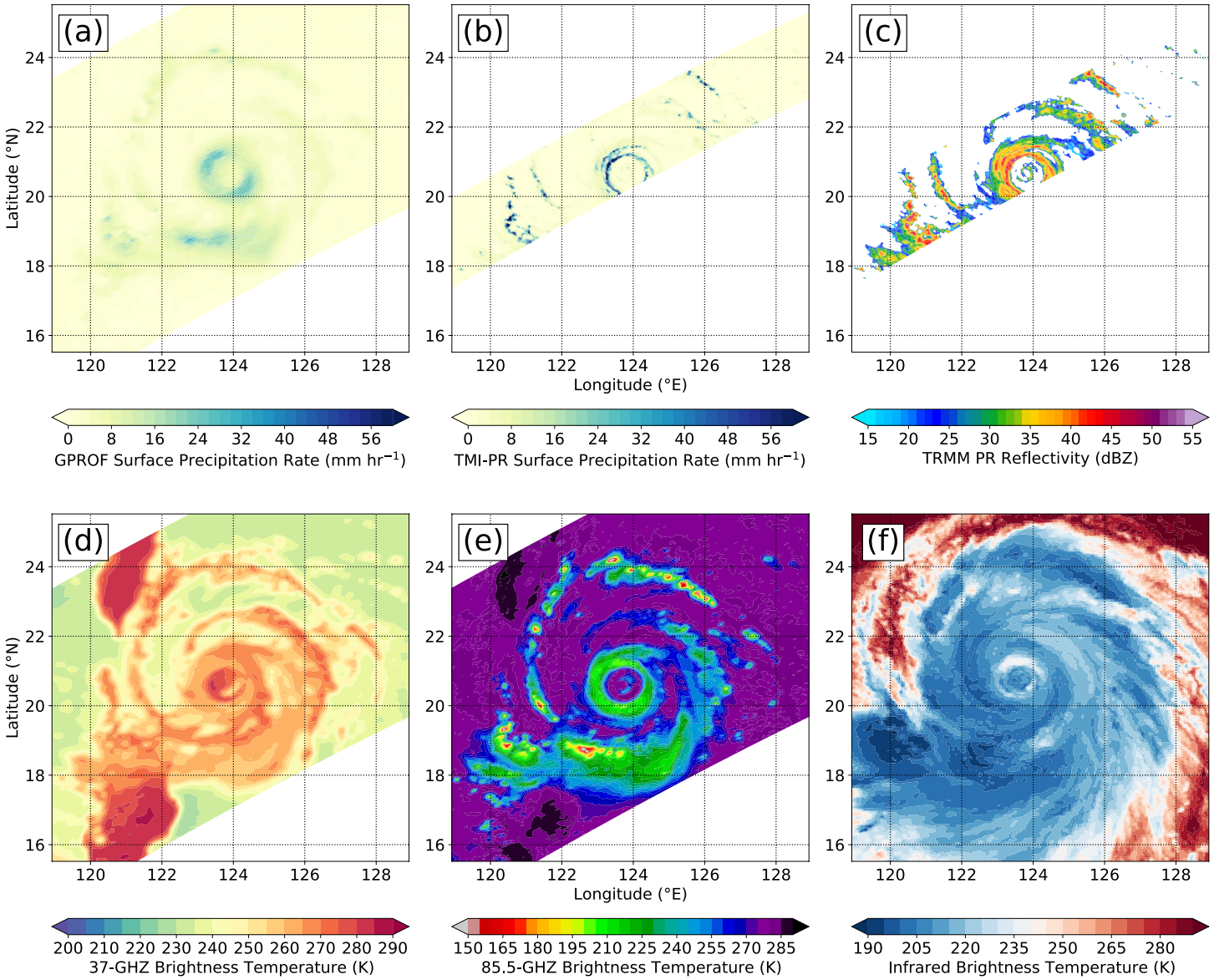

Fig. 2. Example of select satellite variables available in a single satellite overpass file in TC PRIMED, taken from a TRMM overpass of Typhoon Sepat (2007) at 0223:17 UTC 17 Aug 2007. (a) GPROF surface precipitation rate, (b) combined TMI–PR surface precipitation rate, (c) TRMM PR reflectivity at 3-km altitude, (d) 37-GHz vertically polarized microwave brightness temperatures, (e) 85.5-GHz vertically polarized microwave brightness temperatures, and (f) infrared brightness temperatures at 10.8 μm from MTSAT-1R.

using a Bayesian averaging scheme over a larger IFOV. However, the GPROF swath is larger than the TRMM PR swath and can observe the rest of the tropical cyclone beyond the TRMM PR swath. The TRMM PR reflectivity field at 3-km altitude shows Typhoon Sepat's decaying inner eyewall, with its secondary eyewall marked by a high ring of reflectivity (Fig. 2c).

To investigate the distribution of convection in Typhoon Sepat, researchers can use the various satellite proxies available in TC PRIMED. For example, in the 37-GHz microwave frequency, liquid precipitation produces warmer brightness temperatures (TBs) relative to a radiometrically colder ocean surface. However, researchers must practice caution when analyzing 37-GHz TBs, as land can also produce warmer TBs due to its higher emissivity relative to the ocean, while large precipitation-sized ice particles produced in deep convection (e.g., graupel) can scatter low-level emissions in this frequency to produce depressed TBs. Therefore, Fig. 2d shows the general location of liquid precipitation in Typhoon Sepat, with embedded local minima in TB showing the location of stronger convection (e.g., around 18.75°N, 123°E).

In the 85.5–91.665-GHz passive microwave frequencies, the large precipitation-sized ice particles in deep convection scatter terrestrial radiation more distinctly, with low TBs in this frequency most often indicating the presence of deep convection. In the IR, low TBs indicate the presence of cold cirrus ice crystals at cloud top, which are often produced by deep convection. However, cirrus ice crystals are small and do not usually produce precipitation that reaches the surface. Therefore, the low TBs in the microwave ice-scattering frequencies collocate more closely with deep convection, as the swirling winds of the tropical cyclone advect cold cirrus ice crystals away from the source convection. The application of both ice-scattering and IR observations in Typhoon Sepat is shown in Figs. 2e and 2f.

While Fig. 2 demonstrates TC PRIMED's capability to provide a multivariable view of the storm from just a single file, we demonstrate how researchers can also generate a more extensive composite analysis to provide a long-term, globally consistent picture of the distribution of precipitation and convection in tropical cyclones. The composite analysis includes mean GPROF surface precipitation rate, polarization-corrected TBs (PCT) in the ice-scattering frequencies (85.5–91.665 GHz, hereafter IPCTs for brevity), and IR TBs. PCTs combine the horizontal and vertical polarization passive microwave TBs to remove ambiguities produced by varying surface emissivities. We use the equation derived and coefficients recommended in Cecil and Chronis (2018) for the IPCTs.

We composite storms that 1) reached at least category 1 intensity on the Saffir–Simpson hurricane wind scale (65 kt; 33 m s^{-1}) in their lifetime, 2) were at least 200 km away from land and major islands at the time of the passive microwave overpass, and 3) occurred in the North Atlantic, eastern, central, or western North Pacific, or the north Indian Ocean basins. We do not include storms in the Southern Hemisphere since the shear-relative distribution of their precipitation field mirrors that of the Northern Hemisphere storms about the vertical shear vector. For each passive microwave overpass, we bin the available passive microwave and unique IR observations 1) in 6-hourly intervals within ±72 h of the first occurrence of a storm's lifetime maximum intensity and 2) into shear-relative quadrants: upshear right (UR), downshear right (DR), downshear left (DL), and upshear left (UL) following Corbosiero and Molinari (2002).

We linearly interpolate to the passive microwave observation time the distance-to-land values from the best track section of the environmental file and the shear heading values from the diagnostics section. We make no distinction between the different shear magnitudes at the different observation times, nor do we make a distinction between the different intensity trends prior to and after the first occurrence of lifetime maximum intensity. However, for reference, we include the 25th percentile, median, and 75th percentile of their intensity normalized by their lifetime maximum intensity. We use normalized intensity since the lifetime maximum intensity can range from a category 1 to a category 5 storm on the Saffir–Simpson hurricane wind scale.

We scale our observations using the R5-based scaling factor to account for the differences in tropical cyclone size. To obtain the scaling factor, we interpolate the R5 value and relevant parameters to the observation time. In our composite, we bin the satellite variables in 50-km scaled radius bins (R^*). The composite analysis includes only storms with maximum intensity above 34 kt at the observation time, since weaker storms tend to have an extremely large scaled radius relative to its physical radius.

We composite the IPCTs and derived precipitation rates from the conical-scanning AMSR-E, AMSR2, GMI, SSM/I, SSMIS, and TMI sensors in TC PRIMED. Yang et al. (2014) showed significant differences in scene TBs due to the differences in the observing frequencies (i.e., 85.5 vs 89.0 GHz). However, we conducted a simple comparative analysis of AMSR2, SSMIS, and TMI observations from Hurricane Nadine (2012) and found similar IPCT bulk statistics between the different observing frequencies of the different sensors (not shown). Conversely, the resolution of the sensor significantly affects the retrieved precipitation rates, with lower-resolution sensors recording lower retrieved precipitation rates due to its larger IFOV that observes a larger area and misses small, localized precipitation maxima (not shown).

In addition, in conducting this composite analysis with and without the lower-resolution sensors (SSM/I and SSMIS), we found lower mean retrieved precipitation rates in the composite with the lower-resolution sensors. However, neither the differences in IPCTs due to the differences in observing frequencies nor the differences in retrieved precipitation rates due to the differences in IFOV alter the conclusion of this simple demonstrative composite analysis. Therefore, we present the composites that include observations from the lower-resolution sensors. Similarly, we combine the IR TBs from the 8-km HURSAT and the 4-km RAMMB/CIRA data, since separately the composites yield the same conclusion. Figures 3–5 show the respective shear-relative mean and standard deviation of surface precipitation rate, IPCTs, and IR TBs relative to the tropical cyclone lifetime maximum intensity.

The mean rate and radial extent of precipitation gradually increase prior to lifetime maximum intensity in all quadrants, except DL where the radial extent is relatively constant (Fig. 3). At around lifetime maximum intensity, the mean precipitation rate maximizes in each quadrant. The largest radial extent of precipitation occurs in DL, followed by UL and DR, and UR. After the lifetime maximum intensity, around half of the storms in the composite remain relatively strong, with intensities above 60% of their lifetime maximum intensity at 72 h after lifetime maximum intensity. While their mean rate and radial extent of precipitation continue to be large in the DL quadrant, mean rate and radial extent of precipitation diminishes in the DR, UL, and UR quadrants.

The evolution of convection relative to lifetime maximum intensity is similar to the evolution of precipitation, as denoted by the colder TBs in the IPCT and IR composites. The mean TBs grow increasingly colder while the radial extent of colder TB values expands in all quadrants prior to lifetime maximum intensity, except DL where the radial extent is relatively constant (Figs. 4 and 5). At around lifetime maximum intensity, the intensity and radial extent of convection reaches a maximum. The location and intensity of convection are better shown in the IPCTs compared to the IR TBs due to the advection of cirrus ice crystals away from the primary location of convection by the tropical cyclone swirling winds. Following lifetime maximum intensity, the radial extent of colder TBs continues to be large in the DL quadrant, with a decreasing radial extent in the other quadrants that is most pronounced in the UL and UR quadrants. However, while large precipitation rates lingered after the lifetime maximum intensity, particularly in the DL quadrant (Fig. 3), convective intensity denoted by cold TBs did not linger as long, indicating that the large precipitation rates may come from stratiform precipitation.

The evolution of convection and precipitation are consistent with our current understanding of the tropical cyclone life cycle. Convection (and subsequently precipitation rate) intensifies

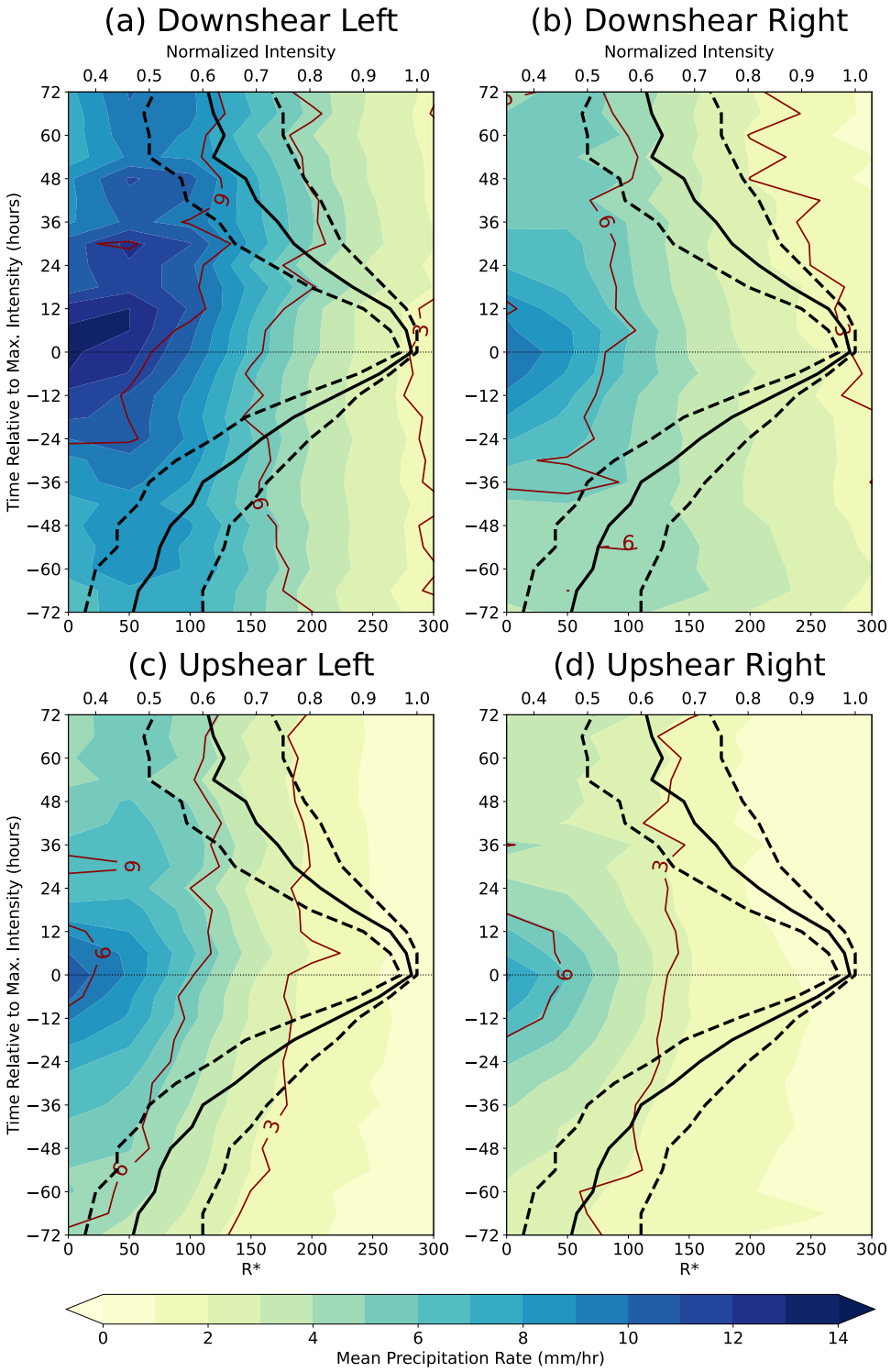

Fig. 3. Shear-relative mean GPROF surface precipitation rate (shading) and standard deviation (dark red contours) for the (a) downshear-left, (b) downshear-right, (c) upshear-left, and (d) upshear-right quadrants. The black solid line shows the median normalized intensity, while the black dashed lines show the 25th and 75th percentiles of normalized intensity. The bottom *x* axes denote the scaled radius, the top *x* axes denote the normalized intensity values, and the *y* axes denote time in hours relative to the first occurrence of storm lifetime maximum intensity.

prior to the lifetime maximum intensity, reaching some semblance of symmetry at around lifetime maximum intensity. After the lifetime maximum intensity, convective intensity weakens or convective coverage decreases. In addition, convection and precipitation symmetry decreases, as evident from the prevalence of convective proxies and precipitation in the downshear quadrants. While the tropical cyclones in the composite remain relatively strong

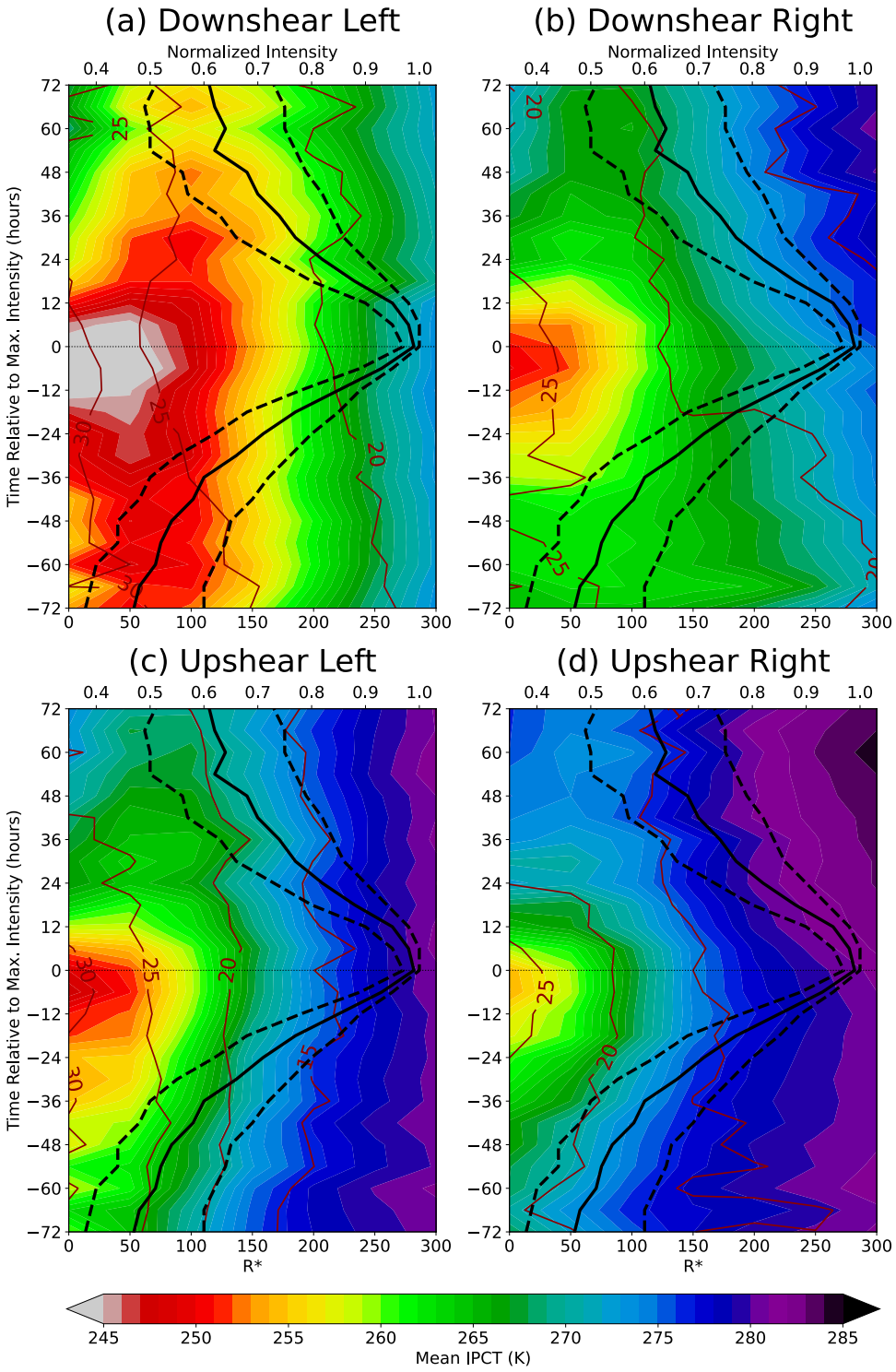

Fig. 4. Shear-relative mean polarization-corrected brightness temperature in the ice-scattering frequencies (85.5–91.665 GHz) (shading) and standard deviation (dark red contours) for the (a) downshear-left, (b) downshear-right, (c) upshear-left, and (d) upshear-right quadrants. The black solid line shows the median normalized intensity, while the black dashed lines show the 25th and 75th percentiles of normalized intensity. The bottom *x* axes denote the scaled radius, the top *x* axes denote the normalized intensity values, and the *y* axes denote time in hours relative to the first occurrence of storm lifetime maximum intensity.

after the lifetime maximum intensity, the decrease in symmetry is the result of increasing shear magnitudes (not shown). Generally, the shear-relative distribution of precipitation and convection in the composite analysis agrees with previous studies (e.g., Chen et al. 2006; Hence and Houze 2012), with preferentially larger radial extent and stronger convection and precipitation rates in the downshear quadrants. However, large standard deviations exist

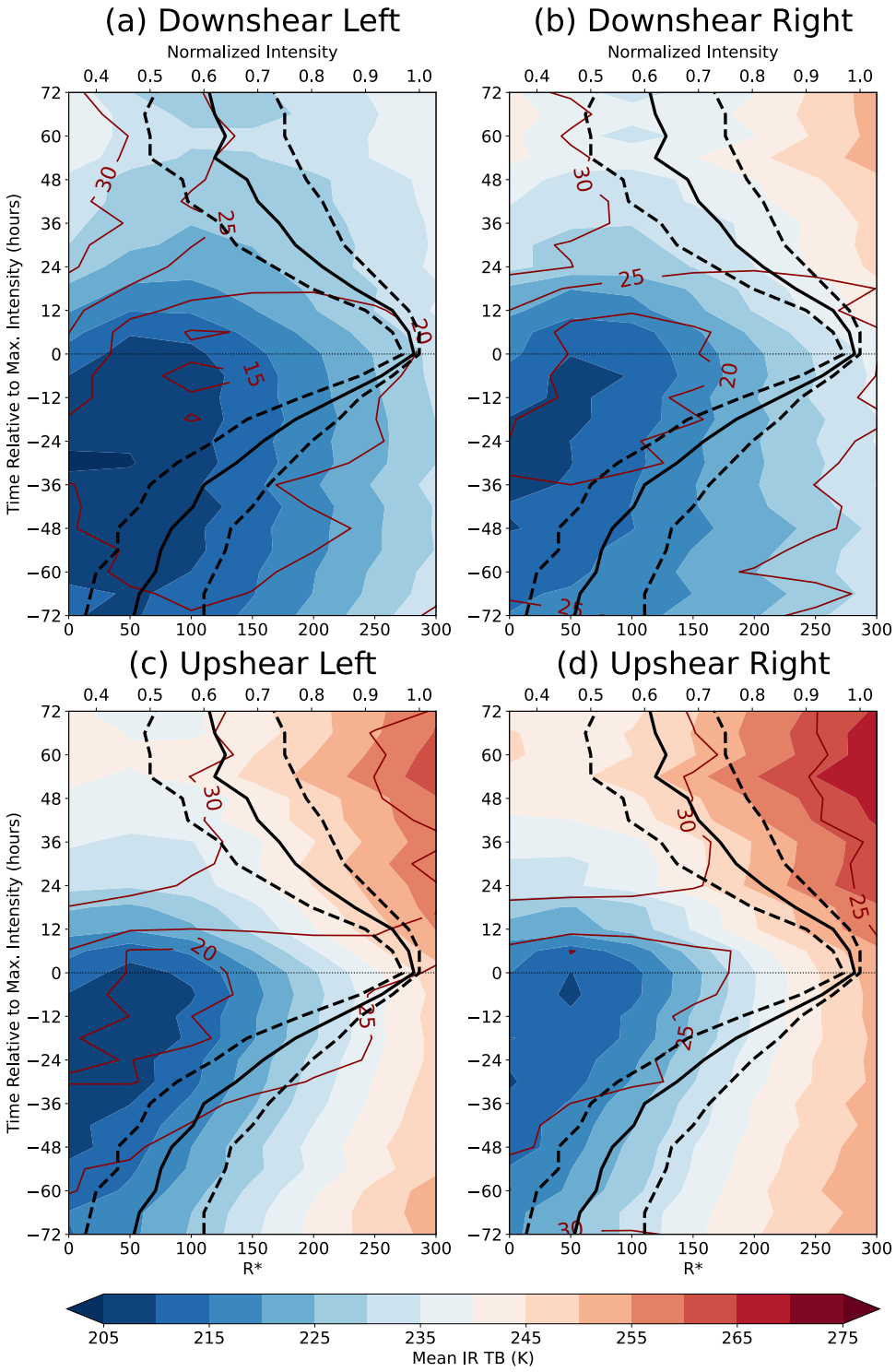

Fig. 5. Shear-relative mean infrared brightness temperature (shading) and standard deviation (dark red contours) for the (a) downshear-left, (b) downshear-right, (c) upshear-left, and (d) upshear-right quadrants. The black solid line shows the median normalized intensity, while the black dashed lines show the 25th and 75th percentiles of normalized intensity. The bottom *x* axes denote the scaled radius, the top *x* axes denote the normalized intensity values, and the *y* axes denote time in hours relative to the first occurrence of storm lifetime maximum intensity.

in all the analyzed fields because we composite observations from sensors with varying IFOVs and did not account for the intensity trends prior to and after the first occurrence of the lifetime maximum intensity.

While our analysis is scientifically straightforward, TC PRIMED makes it simple to conduct. We are able to select the basins, sensors, and variables in TC PRIMED with the understanding

that the data we use come from consistent and well-documented sources. In addition, the standardized file format makes ingesting, compositing, and analyzing the huge number of passive microwave and IR observations in TC PRIMED easy. The scientific community should be able to expand on our analysis with more complex approaches, thus advancing our knowledge of tropical cyclones and improving forecasts.

Conclusions

We have created a long-term, global, research-quality, and open-access dataset of LEO satellite observations of tropical cyclones and associated environmental data called the Tropical Cyclone Precipitation, Infrared, Microwave, and Environmental Dataset (TC PRIMED). TC PRIMED contains tropical cyclone–centric 1) intercalibrated, multichannel, multisensor microwave brightness temperatures, 2) retrieved rainfall from NASA's GPROF, 3) nearly coincident geostationary satellite infrared brightness temperatures and derived metrics, 4) tropical cyclone position and intensity information, 5) ECMWF fifth-generation reanalysis fields and derived environmental diagnostics, and 6) precipitation radar observations from the TRMM and GPM *Core Observatory* satellites. TC PRIMED consists of over 176,000 LEO satellite overpasses of 2,101 storms from 1998 to 2019, with user-friendly files that are compliant with two common metadata conventions. Users can access TC PRIMED data from its official repository through the NOAA National Centers for Environmental Information (NCEI; https://doi.org/10.25921/dmy1-0595) (Razin et al. 2023). There, users can opt to download the full set of TC PRIMED files or browse and download specific TC PRIMED files based on several selection criteria that include but are not limited to sensor type, storm lifetime maximum intensity, intensity change rates, and percent overpass coverage. Users can also browse TC PRIMED files on an Amazon Web Service S3 bucket, as part of the NOAA Open Data Dissemination program (https://noaa-nesdis-tcprimed-pds.s3.amazonaws.com/index.html).

In this paper, we summarized the data sources we used and the key processing steps we employed to create TC PRIMED. We provided an example of TC PRIMED data from a TRMM overpass of Typhoon Sepat (2007). To demonstrate TC PRIMED's broader utility, we created a shear-relative composite analysis using the conical-scanning microwave sensors that are available in TC PRIMED. Our composite analysis corroborates what is known about the distribution of convection and precipitation in tropical cyclones. More importantly, our composite analysis demonstrates the huge potential that TC PRIMED presents to the scientific community. By creating TC PRIMED, we have eliminated the tremendous barrier for the scientific community to obtain a large, long-term, global, research-quality, and open-access dataset of LEO satellite observations of tropical cyclones with associated infrared and environmental data—allowing the scientific community to focus solely on research. Future versions of TC PRIMED may include an extension to the dataset period back to 1987 and up to the most recent tropical cyclone season, version updates, and additional variables such as data from the uncalibrated channels that are not currently available and satellite-derived observations.

Acknowledgments. We thank Kate Musgrave for her support during the early stages of TC PRIMED, and Alex Libardoni and Jack Dostalek for their comments on an early version of the manuscript. We would also like to thank the three anonymous reviewers and the editor, Dan Cecil, for their helpful comments and suggestions. This work was supported by Colorado State University's Office of the Vice President of Research, NASA Earth and Space Science Fellowship (NESSF) Funding Number 80NSSC18K1349, and Office of Naval Research Award N000142012069. The scientific results and conclusions, as well as any views or opinions expressed herein, are those of the author(s) and do not necessarily reflect those of NOAA or the Department of Commerce.

Data availability statement. We document the data sources for each component of TC PRIMED in the supplemental document, "TC PRIMED: Data source documentation." Updates on TC PRIMED are available at https://rammb-data.cira.colostate.edu/tcprimed/.

Appendix: Abbreviations and acronyms

List of key abbreviations used in the paper:

3D	Three-dimensional
DL	Downshear left
DR	Downshear right
GEO	Geostationary orbit
IFOV	Instantaneous field of view
IR	Infrared
LEO	Low-Earth orbit
TB	Brightness temperature
UL	Upshear left
UR	Upshear right

List of key acronyms used in the paper:

ACDD-1.3	Attribute Convention for Dataset Discovery version 1.3
AMSR2	Advanced Microwave Scanning Radiometer 2
AMSR-E	Advanced Microwave Scanning Radiometer for Earth Observing System
AMSU-B	Advanced Microwave Sounding Unit-B
ATCF	Automated Tropical Cyclone Forecast System
ATMS	Advanced Technology Microwave Sounder
CF-1.7	Climate and Forecast version 1.7
CIRA	Cooperative Institute for Research in the Atmosphere
CSU	Colorado State University
DOI	Digital Object Identifier
DPR	(GPM) Dual-Frequency Precipitation Radar
ECMWF	European Centre for Medium-Range Weather Forecasting
ERA5	ECMWF reanalysis version 5
GMI	GPM Microwave Imager
GPM	Global Precipitation Measurement
GPROF	Goddard Profiling Algorithm
HURSAT	Hurricane Satellite Data
MHS	Microwave Humidity Sounder
NASA	National Aeronautics and Space Administration
PR	(TRMM) Precipitation Radar
RAMMB	Regional and Mesoscale Meteorology Branch
SHIPS	Statistical Hurricane Intensity Prediction Scheme
SSM/I	Special Sensor Microwave Imager
SSMIS	Special Sensor Microwave Imager/Sounder
TMI	TRMM Microwave Imager
TRMM	Tropical Rainfall Measuring Mission

References

Alvey, G. R., III, J. Zawislak, and E. Zipser, 2015: Precipitation properties observed during tropical cyclone intensity change. *Mon. Wea. Rev.*, **143**, 4476–4492, https://doi.org/10.1175/MWR-D-15-0065.1.

Awaka, J., M. Le, V. Chandrasekar, N. Yoshida, T. Higashiuwatoko, T. Kubota, and T. Iguchi, 2016: Rain type classification algorithm module for GPM Dual-Frequency Precipitation Radar. *J. Atmos. Oceanic Technol.*, **33**, 1887–1898, https://doi.org/10.1175/JTECH-D-16-0016.1.

Berg, W., and Coauthors, 2016: Intercalibration of the GPM microwave radiometer constellation. *J. Atmos. Oceanic Technol.*, **33**, 2639–2654, https://doi.org/10.1175/JTECH-D-16-0100.1.

Brown, P. J., C. D. Kummerow, and D. L. Randel, 2016: Hurricane GPROF: An optimized ocean microwave rainfall retrieval for tropical cyclones. *J. Atmos. Oceanic Technol.*, **33**, 1539–1556, https://doi.org/10.1175/JTECH-D-15-0234.1.

Cecil, D. J., and T. Chronis, 2018: Polarization-corrected temperatures for 10-, 19-, 37-, and 89-GHz passive microwave frequencies. *J. Appl. Meteor. Climatol.*, **57**, 2249–2265, https://doi.org/10.1175/JAMC-D-18-0022.1.

Chen, S. S., J. A. Knaff, and F. D. Marks Jr., 2006: Effects of vertical wind shear and storm motion on tropical cyclone rainfall asymmetries deduced from TRMM. *Mon. Wea. Rev.*, **134**, 3109–3208, https://doi.org/10.1175/MWR3245.1.

Corbosiero, K. L., and J. Molinari, 2002: The effects of vertical wind shear on the distribution of convection in tropical cyclones. *Mon. Wea. Rev.*, **130**, 2110–2123, https://doi.org/10.1175/1520-0493(2002)130<2110:TEOVWS>2.0.CO;2.

Cossuth, J. H., 2014: Exploring a comparative climatology of tropical cyclone core structures. Ph.D. dissertation, Dept. of Earth Ocean and Atmospheric Science, Florida State University, 185 pp.

DeMaria, M., and J. Kaplan, 1994: A Statistical Hurricane Intensity Prediction Scheme (SHIPS) for the Atlantic Basin. *Wea. Forecasting*, **9**, 209–220, https://doi.org/10.1175/1520-0434(1994)009<0209:ASHIPS>2.0.CO;2.

——, M. Mainelli, L. K. Shay, J. A. Knaff, and J. Kaplan, 2005: Further improvements to the Statistical Hurricane Intensity Prediction Scheme (SHIPS). *Wea. Forecasting*, **20**, 531–543, https://doi.org/10.1175/WAF862.1.

Grecu, M., W. S. Olson, S. J. Munchak, S. Ringerud, L. Liao, Z. Haddad, B. L. Kelley, and S. F. McLaughlin, 2016: The GPM combined algorithm. *J. Atmos. Oceanic Technol.*, **33**, 2225–2245, https://doi.org/10.1175/JTECH-D-16-0019.1.

Harnos, D. S., and S. W. Nesbitt, 2011: Convective structure in rapidly intensifying tropical cyclones as depicted by passive microwave measurements. *Geophys. Res. Lett.*, **38**, L07805, https://doi.org/10.1029/2011GL047010.

Hawkins, J. D., T. F. Lee, J. Turk, C. Sampson, J. Kent, and K. Richardson, 2001: Real-time internet distribution of satellite products for tropical cyclone reconnaissance. *Bull. Amer. Meteor. Soc.*, **82**, 567–578, https://doi.org/10.1175/1520-0477(2001)082<0567:RIDOSP>2.3.CO;2.

Hence, D. A., and R. A. Houze Jr., 2012: Vertical structure of tropical cyclone rainbands as seen by the TRMM Precipitation Radar. *J. Atmos. Sci.*, **69**, 2644–2661, https://doi.org/10.1175/JAS-D-11-0323.1.

Hersbach, H., and Coauthors, 2018a: ERA5 hourly data on pressure levels from 1979 to present. CS3S CDS, accessed 31 July 2020, https://doi.org/10.24381/cds.bd0915c6.

——, and Coauthors, 2018b: ERA5 hourly data on single levels from 1979 to present. C3S CDS, accessed 31 July 2020, https://doi.org/10.24381/cds.adbb2d47.

——, and Coauthors, 2020: The ERA5 global reanalysis. *Quart. J. Roy. Meteor. Soc.*, **144**, 1999–2049, https://doi.org/10.1002/qj.3803.

Hodges, K., A. Cobb, and P. L. Vidale, 2017: How well are tropical cyclones represented in reanalysis datasets? *J. Climate*, **30**, 5243–5264, https://doi.org/10.1175/JCLI-D-16-0557.1.

Hou, A. Y., and Coauthors, 2014: The Global Precipitation Measurement mission. *Bull. Amer. Meteor. Soc.*, **95**, 701–722, https://doi.org/10.1175/BAMS-D-13-00164.1.

Hristova-Veleva, S. M., and Coauthors, 2020: An eye on the storm: Integrating a wealth of data for quickly advancing the physical understanding and forecasting of tropical cyclones. *Bull. Amer. Meteor. Soc.*, **101**, E1718–E1742, https://doi.org/10.1175/BAMS-D-19-0020.1.

Jiang, H., C. Liu, and E. J. Zipser, 2011: A TRMM-based tropical cyclone cloud and precipitation feature database. *J. Appl. Meteor. Climatol.*, **50**, 1255–1274, https://doi.org/10.1175/2011JAMC2662.1.

Jones, T. A., D. Cecil, and M. DeMaria, 2006: Passive-microwave-enhanced Statistical Hurricane Intensity Prediction Scheme. *Wea. Forecasting*, **21**, 613–635, https://doi.org/10.1175/WAF941.1.

Knaff, J. A., S. P. Longmore, and D. A. Molenar, 2014: An objective satellite-based tropical cyclone size climatology. *J. Climate*, **27**, 455–476, https://doi.org/10.1175/JCLI-D-13-00096.1.

——, C. J. Slocum, K. D. Musgrave, C. R. Sampson, and B. R. Strahl, 2016: Using routinely available information to estimate tropical cyclone wind structure. *Mon. Wea. Rev.*, **144**, 1233–1247, https://doi.org/10.1175/MWR-D-15-0267.1.

——, C. R. Sampson, and G. Chirokova, 2017: A global statistical–dynamical tropical cyclone wind radii forecast scheme. *Wea. Forecasting*, **32**, 629–644, https://doi.org/10.1175/WAF-D-16-0168.1.

——, C. J. Slocum, and K. D. Musgrave, 2019: Quantification and exploration of diurnal oscillations in tropical cyclones. *Mon. Wea. Rev.*, **147**, 2105–2121, https://doi.org/10.1175/MWR-D-18-0379.1.

——, and Coauthors, 2021: Estimating tropical cyclone surface winds: Current status, emerging technologies, historical evolution, and a look to the future. *Trop. Cyclone Res. Rev.*, **10**, 125–150, https://doi.org/10.1016/j.tcrr.2021.09.002.

Knapp, K. R., 2008: Hurricane Satellite (HURSAT) data sets: Low Earth orbit infrared and microwave data. *28th Conf. on Hurricanes and Tropical Meteorology*, Orlando, FL, Amer. Meteor. Soc., 4B.4, https://ams.confex.com/ams/28Hurricanes/techprogram/paper_138402.htm.

——, and J. Kossin, 2007: New global tropical cyclone data from ISCCP B1 geostationary satellite observations. *J. Appl. Remote Sens.*, **1**, 013505, https://doi.org/10.1117/1.2712816.

Kummerow, C., W. Barnes, T. Kozu, J. Shiue, and J. Simpson, 1998: The Tropical Rainfall Measuring Mission (TRMM) sensor package. *J. Atmos. Oceanic Technol.*, **15**, 809–817, https://doi.org/10.1175/1520-0426(1998)015<0809:TTRMMT>2.0.CO;2.

——, D. L. Randel, M. Kulie, N.-Y. Wang, R. Ferraro, S. J. Munchak, and V. Petkovic, 2015: The evolution of the Goddard Profiling Algorithm to a fully parametric scheme. *J. Atmos. Oceanic Technol.*, **32**, 165–176, https://doi.org/10.1175/JTECH-D-15-0039.1.

Landsea, C. W., and J. L. Franklin, 2013: Atlantic Hurricane Database uncertainty and presentation of a new database format. *Mon. Wea. Rev.*, **141**, 3576–3592, https://doi.org/10.1175/MWR-D-12-00254.1.

——, G. A. Vecchi, L. Bengtsson, and T. R. Knutson, 2010: Impact of duration thresholds on Atlantic tropical cyclone counts. *J. Climate*, **23**, 2508–2519, https://doi.org/10.1175/2009JCLI3034.1.

Lonfat, M., F. D. Marks Jr., and S. S. Chen, 2004: Precipitation distribution in tropical cyclones using the Tropical Rainfall Measuring Mission (TRMM) Microwave Imager: A global perspective. *Mon. Wea. Rev.*, **132**, 1645–1660, https://doi.org/10.1175/1520-0493(2004)132<1645:PDITCU>2.0.CO;2.

Marchok, T., 2021: Important factors in the tracking of tropical cyclones in operational models. *J. Appl. Meteor. Climatol.*, **60**, 1265–1284, https://doi.org/10.1175/JAMC-D-20-0175.1.

NASA Earthdata, 2021: Data processing levels. Accessed 4 November 2021, https://earthdata.nasa.gov/collaborate/open-data-services-and-software/data-information-policy/data-levels.

Olson, W. S., and Coauthors, 2018: GPM combined radar-radiometer precipitation (version 5). NASA Algorithm Theoretical Basis Doc., 68 pp.

RAMMB, 2020: SHIPS: Statistical tropical cyclone intensity forecast technique development—Developmental data. Accessed 3 April 2020, https://rammb.cira.colostate.edu/research/tropical_cyclones/ships/developmental_data.asp.

Razin, M. N., C. J. Slocum, J. A. Knaff, and P. J. Brown, 2023: Tropical Cyclone Precipitation, Infrared, Microwave, and Environmental Dataset (TC PRIMED),

v01r00. NOAA National Centers for Environmental Information, https://doi.org/10.25921/dmy1-0595.

Rozoff, C. M., C. S. Velden, J. Kaplan, and A. J. Wimmers, 2015: Improvements in probabilistic prediction of tropical cyclone rapid intensification with passive microwave observations. *Wea. Forecasting*, **30**, 1016–1038, https://doi.org/10.1175/WAF-D-14-00109.1.

Sampson, C. R., and A. J. Schrader, 2000: The Automated Tropical Cyclone Forecasting System (version 3.2). *Bull. Amer. Meteor. Soc.*, **81**, 1231–1240, https://doi.org/10.1175/1520-0477(2000)081<1231:TATCFS>2.3.CO;2.

Slocum, C. J., M. N. Razin, J. A. Knaff, and J. P. Stow, 2022: Does ERA5 mark a new era for resolving the tropical cyclone environment? *J. Climate*, **35**, 7147–7164, https://doi.org/10.1175/JCLI-D-22-0127.1.

Wingo, M. T., and D. J. Cecil, 2010: Effects of vertical wind shear on tropical cyclone precipitation. *Mon. Wea. Rev.*, **138**, 645–662, https://doi.org/10.1175/2009MWR2921.1.

Yang, S., J. Hawkins, and K. Richardson, 2014: The improved NRL tropical cyclone monitoring system with a unified microwave brightness temperature calibration scheme. *Remote Sens.*, **6**, 4563–4581, https://doi.org/10.3390/rs6054563.